Proceedings 10th NUMGE 2023
10th European Conference on Numerical Methods in Geotechnical Engineering
Zdravkovic L, Kontoe S, Taborda DMG, Tsiampousi A (eds)

https://doi.org/10.53243/NUMGE2023-128

Shear strength reduction analysis and its usage in slope stability with unconfined seepage

S. Sysala[1], F. Tschuchnigg[2], E. Hrubešová[3], Z. Michalec[1]

[1]*Institute of Geonics of the Czech Academy of Sciences, Ostrava, Czech Republic*
[2]*Institute of Soil Mechanics, Foundation Engineering and Computational Geotechnics, Graz University of Technology, Graz, Austria*
[3]*Faculty of Civil Engineering, VSB - Technical University of Ostrava, Ostrava, Czech Republic*

Dedication: This paper is dedicated to the late Professor Scott Sloan. The second author has significantly benefited from discussions with Scott on advantages and disadvantages of limit analysis, a method he pioneered with his co-workers.

ABSTRACT: In this contribution, we introduce the shear strength reduction analysis built on an optimization definition and Davis approximations of the non-associated Mohr-Coulomb plastic flow rule. This optimization framework has many common features with limit analysis. For example, it is possible to analyse duality between static and kinematic principles or use more advanced numerical methods. A solution concept based on a regularization method, standard finite elements, continuation Newton method and mesh adaptivity is used. The suggested shear strength reduction analysis is used for a case study of a heterogeneous embankment dam. For the comparison of results, the Plaxis code is considered.

Keywords: slope stability; shear strength reduction; optimization; finite elements; unconfined seepage

1 INTRODUCTION

The shear strength reduction method (SSRM) is a conventional method in slope (dam, embankment) stability enabling to determine the factor of safety (FoS) and related failure zones. Its basic variant arises from the elastic-perfectly plastic model containing the Mohr-Coulomb yield criterion and is based on a displacement variant of the finite element method (FEM).

The non-associated plastic flow rule is frequently used in geotechnical practice to control the inelastic volume changes of soils. On the other hand, the standard SSRM for the non-associated plasticity does not work well in some cases, especially if higher values of the effective friction angle and lower values of the dilatancy angle are considered. In such cases, spurious numerical oscillations and strong dependence on mesh density may appear within the computation of FoS, see (Tschuchnigg at al., 2015a; Tschuchnigg et al., 2015b).

To suppress this drawback, the so-called Davis approach (see e.g. (Sloan, 2013)) was extended from limit analysis to SSRM. Its idea is to approximate the non-associated model by the associated one. In particular, three different Davis' modifications for SSRM was proposed and combined with an iterative limit analysis procedure in (Tschuchnigg at al., 2015a; Tschuchnigg et al., 2015b; Tschuchnigg et al., 2015c). For more advanced theoretical and numerical analyses of the modified SSRM, its optimization framework (OPT-MSSRM) was recently developed in (Sysala et al., 2021). Similarly as in limit analysis, the optimization theory is based on rigid plasticity and the duality between the static and kinematic settings of the problem. Water pore pressure may also be incorporated to the optimization framework, see (Sysala et al., 2023).

The rest of this contribution is organized as follows. In Section 2, the OPT-MSSRM is introduced and a convenient solution concept is briefly recapitulated. In Section 3, implementation details to in-house codes in Matlab are mentioned. Sections 4 and 5 are devoted to the strength reduction analysis of two case studies of heterogeneous embankments. OPT-MSSRM implemented in Matlab is compared with Plaxis results. Concluding remarks can be found in Section 6.

2 OPTIMIZATION VARIANT OF MSSRM

The optimization variant of the modified shear strength reduction method (OPT-MSSRM) reads as:

FoS = supremum of $\lambda \geq 0$ *subject to*

$$\begin{cases} -\operatorname{div} \boldsymbol{\sigma} = \boldsymbol{F} \text{ in } \Omega, \quad \boldsymbol{\sigma n} = \boldsymbol{f} \text{ on } \partial\Omega_f \\ \boldsymbol{\sigma} = \boldsymbol{\sigma}' - \theta \boldsymbol{I} \text{ in } \Omega, \\ \Phi(q(\lambda); \boldsymbol{\sigma}') \leq 0 \text{ in } \Omega, \end{cases} \tag{1}$$

Here, $\boldsymbol{\sigma}$, $\boldsymbol{\sigma}'$ denote the total and effective Cauchy stress tensors, respectively, and θ stands for the water pore pressure. (We use the sign convention with the stresses positive in tension and the pore pressures positive in compression.) Next, Ω is a bounded domain in 2D or 3D representing an investigated body (a slope or an embankment). The boundary of Ω and its outward unit normal are denoted as $\partial\Omega$ and $\boldsymbol{n}$, respectively. To simplify the setting the problem, we assume that the boundary $\partial\Omega$ can be split into two disjoint parts $\partial\Omega_f$ and $\partial\Omega_v$ where different boundary conditions are considered. Namely, the surface force $\boldsymbol{f}$ acts on $\partial\Omega_f$ and the body is assumed to be fixed on $\partial\Omega_v$. The volume force is denoted as $\boldsymbol{F}$ and it usually represents a soil unit weight of a soil material, which can depend on the degree of saturation.

The function Φ represents the Mohr-Coulomb yield criterion. For purposes of theoretical analysis of OPT-MSSRM, the following form of this criterion was suggested in (Sysala et al., 2021):

$$\Phi(q(\lambda);\boldsymbol{\sigma}') = (\sigma'_1 - \sigma'_1)\sqrt{q^2(\lambda) + \tan^2\phi'} + (\sigma'_1 + \sigma'_3)\tan\phi' - 2\,c', \qquad (2)$$

where σ'_1, σ'_3 stand for the maximal and minimal principle stresses, and ϕ', c' denote the effective friction angle and the effective cohesion, respectively. Using the scalar function q and its variable λ, we reduce the strength parameters ϕ', c'. If the associated plastic flow rule is considered then $q(\lambda) = \lambda$. For the non-associated model, the function q represents the so-called Davis modifications of SSRM suggested in (Tschuchnigg et al. 2015a, 2015b, 2015c). In this paper, we shall work with the Davis B approach, for the sake of simplicity. The corresponding function q was introduced in (Sysala et al. 2021):

$$q(\lambda) = \frac{\sqrt{(\lambda^2+\tan^2\psi')(\lambda^2+\tan^2\phi')} - \tan\psi'\tan\phi'}{\lambda}, \qquad (3)$$

where ψ' denotes the dilatancy angle. Let us recall that ψ' is mostly lower than ϕ'. If $\psi' = \phi'$ then we arrive at the associated plastic flow rule and the right-hand side in Eq. (3) is equal to λ.

The pore pressure θ is assumed to be given within the stability analysis. Due to this fact, one can eliminate the the total stress and simplify the constraint set in Eq. (1) as follows:

$$\begin{cases} -\operatorname{div}\boldsymbol{\sigma}' = \boldsymbol{F}' \text{ in } \Omega, \ \ \boldsymbol{\sigma n} = \boldsymbol{f}' \ \text{ on } \partial\Omega_f \\ \qquad \Phi(q(\lambda);\boldsymbol{\sigma}') \le 0 \ \text{ in } \Omega, \end{cases} \qquad (4)$$

where $\boldsymbol{F}' = \boldsymbol{F} - \nabla\theta$ and $\boldsymbol{f}' = \boldsymbol{f} + \theta\boldsymbol{n}$.

The optimization problem defined above can be classified as the static principle to OPT-MSSRM. The corresponding dual (kinematic) principle was derived in Sysala et al. (2021) and enables us to define FoS as follows:

$$FoS = \sup_{\lambda\ge 0}\big(\lambda + G(\lambda)\big), \qquad (5)$$

where

$$G(\lambda) = \inf_{\boldsymbol{v}\in V}\Big[\int_\Omega D\big(q(\lambda);\varepsilon(\boldsymbol{v})\big)\,dx - L(\boldsymbol{v})\Big], \qquad (6)$$

$$\varepsilon(\boldsymbol{v}) = \tfrac{1}{2}(\nabla\boldsymbol{v} + (\nabla\boldsymbol{v})^\top), \qquad (7)$$

$$L(\boldsymbol{v}) = \int_\Omega \boldsymbol{F}'.\boldsymbol{v}\,dx + \int_{\partial\Omega_f}\boldsymbol{f}'.\boldsymbol{v}\,ds, \qquad (8)$$

$$D(q(\lambda);\boldsymbol{\varepsilon}) = \sup_{\substack{\boldsymbol{\sigma}\in\mathbb{R}^{3\times3}_{sym} \\ \Phi(q(\lambda);\boldsymbol{\sigma})\le 0}} \boldsymbol{\sigma} : \boldsymbol{\varepsilon}\,. \qquad (9)$$

Here, V is a functional space of admissible velocity fields vanishing on the part $\partial\Omega_v$ of the boundary a D is the local dissipation function. This function is not finite-valued for any $\boldsymbol{\varepsilon}$ due to the fact that the Mohr-Coulomb pyramid is unbounded. Hence, the inf-problem in Eq. (6) contains hidden constraints.

The solution concept presented in (Sysala et al. 2021, 2023) is based on a smooth approaximation (regularization) of the function D. Consequently, standard finite elements, continuation Newton method and mesh adaptivity are used to determine the safety factor λ^* as much as accurately.

Let us note that problems (1) and (6) could be alternatively solved by methods developed in (Krabbenhoft and Lyamin 2015; Sloan 2013).

3 IMPLEMENTATION DETAILS

The solution concept presented above has been implemented within in-house codes in Matlab. These codes are based on Lagrange finite elements. They have been subsequently developed for various problems of computational plasticity and some of them are available for download, see e.g. (Cermak et al. 2019; Sysala et al. 2017).

For the numerical example studied below, it is necessary to solve at first the steady-state unconfined seepage problem and find the pore pressure θ. We follow the solution concept suggested in (Borja and Kishnani 1991) and enrich it by mesh adaptivity in order to detect unknown phreatic surface more accurately.

Next, we choose 6-noded triangular elements (P2 elements) for kinematic fields in mechanics and even for pore pressures and observe that this choice is sufficient in combination with the mesh refinements. The coarsest mesh is exported from Comsol Multiphysics. Its refinement by adaptive algorithms is done directly in Matlab.

For comparison, we use software Plaxis. It enables to solve the investigated hydro-mechanical stability models by means of the standard SSR methods. For the application of the Davis B approach, a more advanced

iterative procedure has to be used. In the investigated example, 15-noded triangular (P4) elements with a shape function of fourth order are chosen for both displacements and pore pressures. Let us note that meshes used in Plaxis are chosen to be much finer than in Matlab because no mesh adaptivity is applied there.

4 STABILITY OF AN EMBANKMENT DAM

In the first numerical example, we consider a heterogeneous embankment dam founded on flat ground, see Figure 1. The model dimensions considered in the example are 1200 and 500 meters in the horizontal and vertical directions, respectively, and the dam is in the central part of the geometry. The dam and underlying soil consist of the following materials: A - Impervious Core, B - Transition to Dam Fill, C1 - Earth Fill Downstream, C2 - Earth Fill Upstream, RF - Rock Fill, D - Drainage, E - Grout Curtain, and X - Bedrock. More information related to the investigated embankment dam can be found in (Scheikl, 2022; Sysala et al. 2023). We consider a case study with impoundment water level at 60m above ground, see Figure 2.

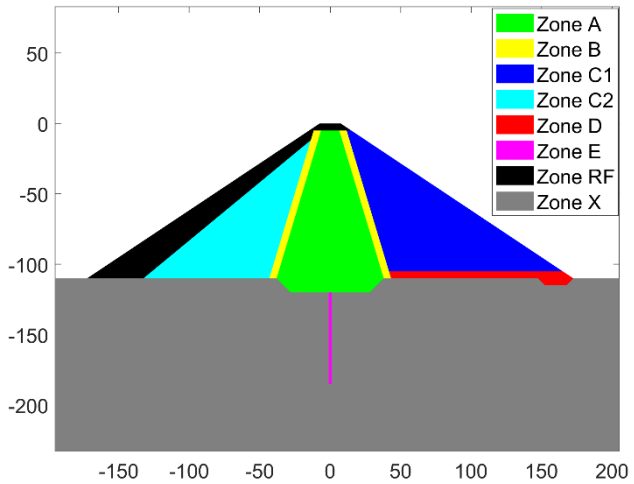

Figure 1. Scheme of a heterogeneous embankment dam on a flat foundation. A detail the foundation is visualized.

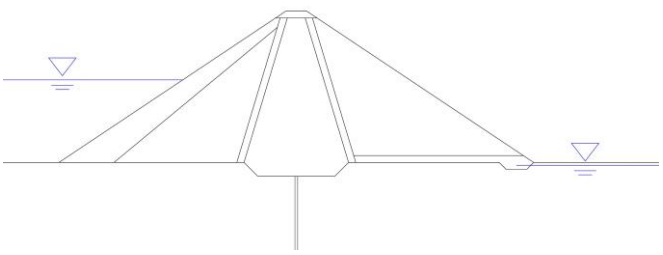

Figure 2. Hydralic conditions with impoundment water level at 60m above ground and groundwater level at 2m below ground.

Material parameters are listed in Table 1. Two different choices of the dilatancy angle are considered and compared. Case A refers to the associated analysis while case NA is related to the non-associated analysis. Let us note that material set NA is of high practical relevance, since information related to the dilatancy angle are often missing in geotechnical reports.

Table 1. Material parameters for the heterogeneous dam and its foundation.

Material	γ [kN/m^3]	c [kPa]	ϕ' [°]	A ψ' [°]	NA ψ' [°]	k [m/s]
A	22	10	25	25	0	1e-9
B	23	0	38	38	0	5e-6
C1	23	0.5	41	41	0	5e-5
C2	23	0.5	40	40	0	5e-5
RF	22	0.5	41	41	0	1e-4
D	21	0.5	41	41	0	5e-4
E	27	75	42	42	42	5e-9
X	27	50	42	42	42	1e-5

The initial mesh for Matlab computations is depicted in Figure 3. We see that the mesh is much finer in the subdomain representing the dam. It consists of 4920 elements. 6-noded elements are considered. The mesh was then refined within the solution of unconfined seepage problem and also within the stability problem.

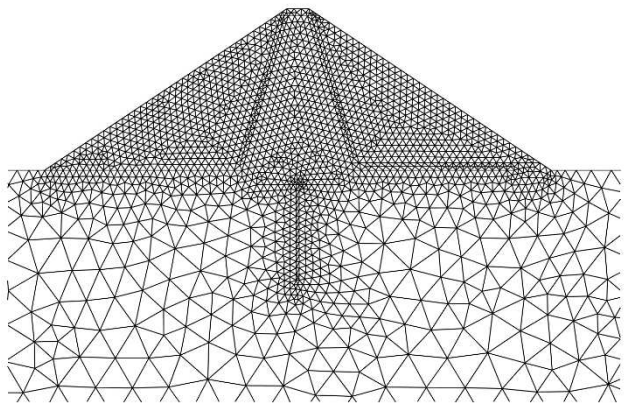

Figure 3. The initial Matlab mesh for the dam problem.

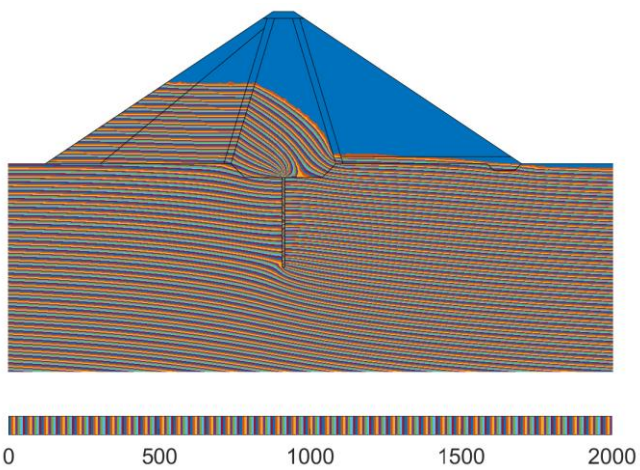

Figure 4. Isolines of the pore pressures for the water level 60m above the ground.

In Figure 4, one can see isolines of computed pore pressures. The blue subdomain is a dry part of the dam.

Consequently, the stability analysis was done. In Figure 5, the failure zone computed in Matlab is depicted. A norm of the incremental deviatoric strain was used for the visualization.

The adaptively refined mesh is shown in Figure 6. We see that it reflects the failure zone and phreatic surface.

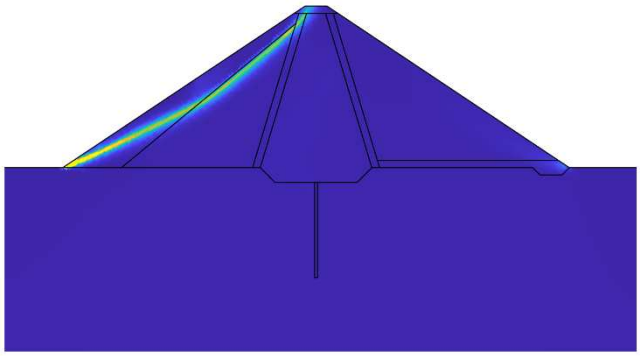

Figure 5. Failure zone computed in Matlab.

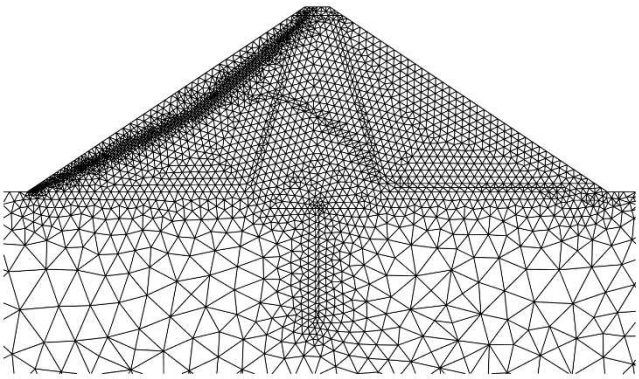

Figure 6. Adaptively refined mesh.

Computed FoS are compared in Table 2.

Table 2. Comparison of FoS for various approaches.

	Matlab	Plaxis
Case A	1.28	1.27
Case NA, Davis B	0.96	< 1.00
Case NA, SSRM	-	1.01-1.10

One can observe the following:

- The dilatancy angle has a significant influence on the results.
- The dam is unstable for the Case NA, Davis B.
- Matlab and Plaxis results are very similar for both the cases although different numerical methods, finite elements and meshes were used.
- Plaxis computation for the case NA and the standard SSRM leads to spurious numerical oscillations (see Figure 7). Consequently, FoS cannot be uniquely determined.

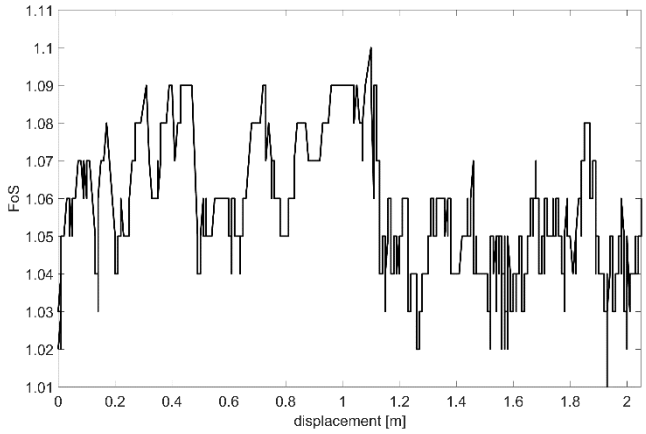

Figure 7. Numerical oscillations observed for the standard SSRM and Case NA within the computational procedure in Plaxis. The x-axis represents displacements at a node on a failing soil mass.

5 STABILITY OF A RIVER EMBANKMENT

The second numerical example is devoted to a case study of a real river embankment in village Lužec (upon the Vltava river, Czech Republic).

The geometry of the embankment and surrounding soil layers are depicted in Figure 8. We distinguish three different soil layers: fluvial clay (cyan), fluvial gravel (green) and weathered claystone (black). The embankment is created by clayey sand (blue). It contains the road (magenta) and the drainage (yellow) with a drainage tile. To represent the tile we prescribe zero water pressure on a central part of the drainage bottom. The length of this part is 10 cm. The river area is located on the right-hand side of the embankment. The height of the flood water level is 22.40m (13 cm below the top of the embankment). Below the river, we assume that the soil is saturated. The groundwater level of the height 15.75m is considered on the left-hand side, that is, in the top part of the green region. Let us note that the geometry is longer on the left-hand side. This is necessary to obtain a realistic distribution of water porous flow. The impermeability conditions are considered at the bottom.

Values of material parameters follow from a Geotechnical report (provided by the embankment designer) and are specified in Table 3.

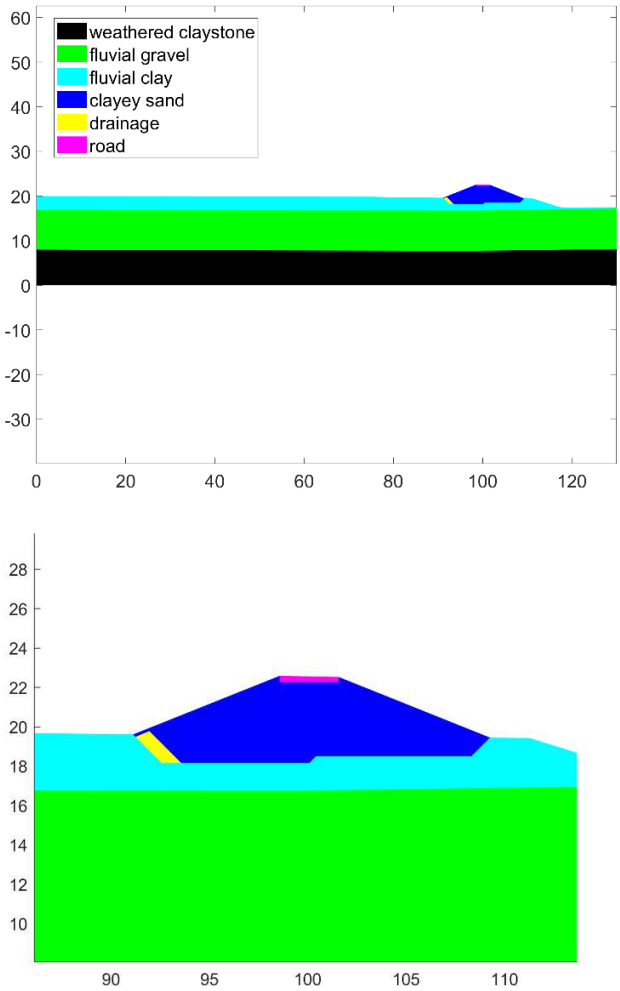

Figure 8. The geometry of the river embankment including details. Dimensions are in meters.

Table 3. Material parameters for the river embankment (FC – fluvial clay, FG – fluvial gravel, WC – weathered claystone, CS – clayey sand, R- road, D - drainage).

Material	$\gamma_{uns}/\gamma_{sat}$ [kN/m^3]	c [kPa]	ϕ' [°]	k [m/day]
FC	21 / 22	7.5	30.25	8.64e-4
FG	19 / 21	1.0	33.00	8.64e+1
WC	21 / 21	14.0	21.00	8.64e-4
CS	19 / 21	1.6	24.00	8.64e-1
R	19 / 19	-	-	-
D	21 / 21	2.0	2.00	8.64e+1

Here, γ_{uns} , γ_{sat} denote the soil unit weights for unsaturated and saturated materials, respectively. Local soil materials were used to build the embankment and thus the sand contains a small amount of fine particles (silt and clay). The values of the dilatancy angle were not available for us (as often the case in practical engineering), therefore, we set $\psi' = 0$ for all materials (Case NA). However, we also consider the associated case (Case A) with $\psi' = \phi'$ in order to analyze the influence of the dilatancy angle.

The initial mesh used for the Matlab computation is depicted in Figure 9. It was created in Comsol Multiphysics and then imported in Matlab. The mesh consists of 1850 elements.

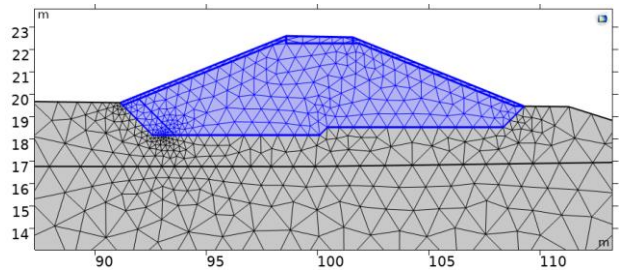

Figure 9. Detail of the initial mesh used for Matlab computation.

First, the unconfined seepage problem is solved. The computed pore pressures are visualized in Figure 10 using isolines. Blue region represents unsaturated part of the embankment. It is worth noticing that the phreatic level increased behind the drainage until the surface. This indicates that the considered drainage causes only a local decrease of the phreatic surface.

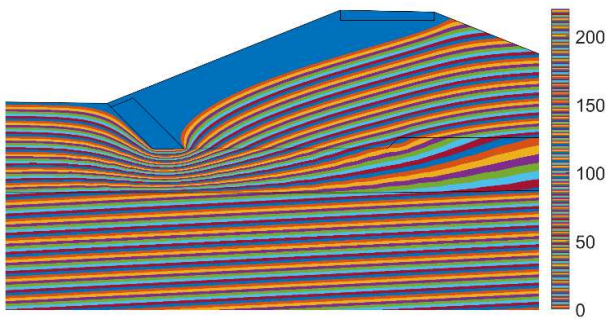

Figure 10. Isolines of the pore pressures for the flood water level.

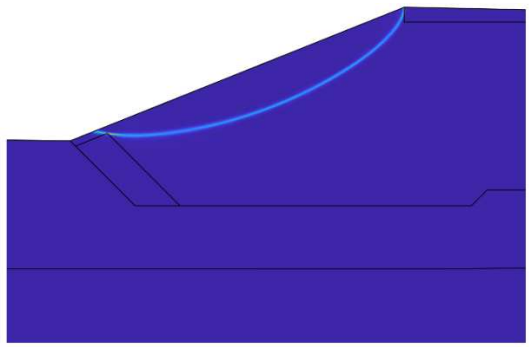

Figure 11. Failure mechanism for the investigated case study of the river embankment.

The consequent stability analysis in Matlab was done by using the Davis B approach. The computed failure zone is depicted in Figure 11 and the corresponding adaptively refined mesh is visualized in Figure 12. One can see that the refined mesh is in accordance with the failure and phreatic surfaces.

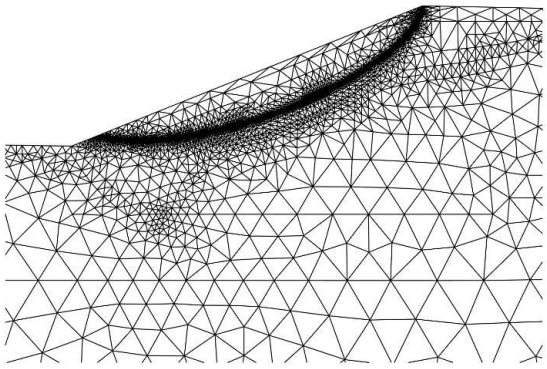

Figure 12. Adaptively refined mesh for the investigated case study of the river embankment.

Computed FoS are compared in Table 4.

Table 4. Comparison of FoS for various approaches.

	Matlab	Plaxis
Case A	1.63	1.64
Case NA, Davis B	1.56	1.58
Case NA, SSRM	-	1.62

One can observe the following:

- The strength parameters of the clayey sand layer have the largest impact on FoS. Since the effective friction angle of this layer is relatively low, the computed FoS are similar for the associated, non-associated and Davis B analyses.
- Matlab and Plaxis results are similar for both the cases although different numerical methods, finite elements and meshes were used.
- No spurious numerical oscillations are observed in Plaxis for the standard SSR method.

6 CONCLUSIONS

We have proposed the OPT-MSSRM method as an alternative to the standard shear strength reduction method. The suggested method is supported by rigorous theory even if the non-associated plastic model is considered. Consequently, numerical analysis of the problem can be done leading to advanced numerical techniques. In particular, we have used the finite element analysis in combination with the regularization method, a Newton-like solver and mesh adaptivity. Due to the usage of local mesh adaptivity.

Next, we have developed the in-house code in Matlab and use it for the solution of heterogeneous embankments with unconfined seepage. The results have been compared with the ones computed in Plaxis.

We have shown that the standard shear strength reduction (in combination with non-associated plasticity) can lead to spurious numerical oscillations (see Figure 7), which are even more pronounced if the finite element mesh is refined. Due to this fact, one cannot uniquely determined FoS or failure zones. Contrary, the Davis B approach is robust with respect to the mesh refinement. Although this approach can be implemented in commercial software packages, its numerical realization is not so straightforward as for the standard approach. Our work can be inspirative for developers of commercial codes.

7 ACKNOWLEDGEMENTS

The research has been supported by European Union's Horizon 2020 research and innovation programme under grant agreement number 847593 and by The Czech Radioactive Waste Repository Authority (SÚRAO) under grant agreement number SO2020-017.

8 REFERENCES

Borja, R.I., Kishnani, S.S. 1991. On the solution of elliptic free-boundary problems via Newton's method. *Computer Methods in Applied Mechanics and Eng*. **88**, 341–361.

Čermák, M., Sysala, S., Valdman, J. 2019. Efficient and flexible MATLAB implementation of 2D and 3D elastoplastic problems. *Applied Mathematics and Computation* **355**, 595–614.

Krabbenhoft, K., Lyamin, A.V. 2015. Strength reduction finite-element limit analysis. *Géotechnique Letters* **5**, 250–253.

Scheikl, M. 2022. Dynamic Finite Element Analyses of the Earthquake Response of Large Embankment Dams. *Master's Thesis*, Graz University of Technology (2022).

Sloan, S.W. 2013. Geotechnical stability analysis. *Géotechnique* **63**, 531–571.

Sysala, S., Čermák, M., Ligurský, T. 2017. Subdifferential-based implicit return-mapping operators in Mohr-Coulomb plasticity. *ZAMM* **97**, 1502–1523.

Sysala, S., Hrubesova, E., Michalec, Z., Tschuchnigg, F. 2021. Optimization and variational principles for the shear strength reduction method. *International Journal for Numerical and Analytical Methods in Geomechanics* **45**, 2388–2407.

Sysala, S., Tschuchnigg, F., Hrubešová, E., Michalec, Z. 2023. Optimization variant of the shear strength reduction method and its usage for stability of embankments with unconfined seepage. *Computers and Structures* **281**, 107033

Tschuchnigg, F., Schweiger, H.F., Sloan, S.W., Lyamin, A.V. and Raissakis, I. 2015a. Comparison of finite-element limit analysis and strength reduction techniques. *Géotechnique* **65**, 249–257.

Tschuchnigg, F., Schweiger, H.F., Sloan, S.W. 2015b. Slope stability analysis by means of finite element limit analysis and finite element strength reduction techniques. Part I: Numerical studies considering non-associated plasticity. *Computers and Geotechnics* **70**, 169–177.

Tschuchnigg, F., Schweiger, H.F., Sloan, S.W. 2015c. Slope stability analysis by means of finite element limit analysis and finite element strength reduction techniques. Part II: Back analyses of a case history. *Computers and Geotechnics* **70**, 178–189.